Study of Radio Channel for Biomedical Sensors in Spacesuits

Mohammed Taj-Eldin
Kansas State University
Department of Electrical and Computer Engineering
Manhattan, KS 66506
(910)545-0131
tajeldin@k-state.edu

William Kuhn
Kansas State University
Department of Electrical and Computer Engineering
Manhattan, KS 66506
(785)532-4649
wkuhn@ksu.edu

Balasubramaniam Natarajan
Kansas State University
Department of Electrical and Computer Engineering
Manhattan, KS 66506
(785)532-4597
bala@ksu.edu

ABSTRACT
Current space suits use conventional wired links to acquire bio-medical sensor data. Replacing these with wireless links would provide a number of operational benefits, but the radio path loss environment must be understood first. In this paper, we study the radio channel of body area networks for space suit applications. Our main findings are that the transmission mechanism follows a coaxial cable model and is approximately 8.5dB/30cm loss at 400 MHz.

Categories and Subject Descriptors
C.2 [**Computer-Communication networks**]: wireless communications, network communications.

General Terms
Measurement, Performance, Experimentation.

Keywords
Coaxial model, on-body propagation, path loss, space suits, wireless body area networks.

1. INTRODUCTION
Wireless body area networks (WBANs) are garnering significant research interest as they enable many applications involving biomedical sensing (e.g., measuring heart rate, blood pressure and body temperature). The FCC has recently allocated a number of different frequency spectrums such as the spectrum between 401 and 406 MHz [1]. In this work, our interest is to understand the WBAN radio channel encountered in a unique application involving astronauts. Monitoring astronaut vital body signs in real time is currently done via a limited number of wired sensors. The benefits of employing WBANs within space suits include (1) weight reduction and protection against mechanical/material wear associated with wiring; and (2) ability to monitor multiple vital signs to better understand the burden of space missions on astronaut health. Therefore, as we look to the future, there exists a compelling need for designing and implementing WBANs within a space suit environment. There have been many studies of signal propagation for body area networks such as [2] and channel characterization for UWB channels [3]. However, to the best of our knowledge, no work has been published for RF signal propagation inside a space suit – an important prerequisite for WBAN design.

In this paper, we take the first step towards designing an intra-space suit WBAN by characterizing the radio channel within the suit. Due to the existence of an outer metallic shield with multiple layers of aluminized mylar in currents suits [4], traditional BAN channel models cannot be directly applied to the intra-suit environment. Our goal is to first understand the basic propagation structure within the space suit. Towards this end, we unitarily consider a small scale model capturing propagation along a human arm within a shielded suit. Then, we will build our analysis, experiments and simulations around the results from this small scale section of the body. The key contributions/finding of this paper is that the transmission model within the space suit does not conform to a circular waveguide propagation model. Rather, the transmission follows a coax propagation model with no lower cutoff frequency.

2. SPACESUIT AND WAVE PROPAGATION MODELS
The space suit used in this study is the EMU spacesuit. This suit is composed of multiple layers [4]: Cooling and Ventilation Garment (CVG) liner, liquid CVG (LCVG) water transport, pressure bladder, and thermal micrometeoroid garment (TMG) cover layers. The outermost Thermal (TMG) segment includes multiple metallic layers of aluminized Mylar. These layers are radio opaque at UHF and above due to the thickness of the metallization used. Although this study is based on the EMU space suit, the analysis and findings are valid for any space suit that has the electrical properties and type of material mentioned above. In this paper, we investigate the propagation characteristics of the channel formed inside this metallic structure at frequencies from 300 kHz to 3 GHz.

2.1 Loaded Circular Waveguide
The cylindrical metal structure of the space suit's outer layers along with the human arm within, motivates the consideration of a loaded circular waveguide propagation model. In this hypothesized model, one can calculate the cutoff frequency based on the TE_{11} mode for propagation as it is typically the dominant propagation mode, see Figure 1(a). The cutoff frequency for this mode can be calculated from:

$$f_{c_{mn}}^{TE} = \frac{\chi'_{mn}}{2\pi a\sqrt{\mu\varepsilon}} \quad (1)$$

BODYNETS 2013, September 30-October 02, Boston, United States

DOI 10.4108/icst.bodynets.2013.253719

where a is the radius of the waveguide. For example, by substituting the speed of light in free-space for $1/\sqrt{\mu\epsilon}$ with $a = 0.095$ meters and χ'_{11}=1.8412 in (1) results in $f_{c_{11}}^{TE}$ = 925 MHz. If the circular waveguide model holds, we anticipate seeing a cutoff frequency between two extreme cases ($f_{c_{11}}^{TE}$ with air dielectric = 976 MHz and $f_{c_{11}}^{TE}$ with full core of human tissue = 158.4 MHz).

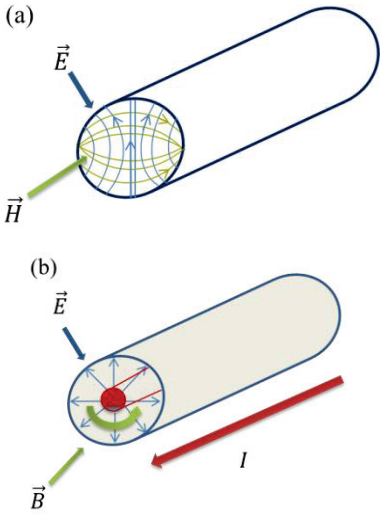

Figure 1. Dominant Mode ($f_{c_{11}}^{TE}$) in (a) circular waveguide [5] and (b) TEM mode in coax model

2.2 Coax Cable Model

Next, we consider a coaxial transmission line model. Figure 1(b) depicts this model. The electric field (E) is normal to the surface of inner conductor (astronaut's arm) and the magnetic field (B) is tangential to the inner and outer surfaces and normal to both the electric field and to the direction of wave propagation.

It should be noted that the transverse electro-magnetic (TEM) fields illustrated in Figure 1(b) represent ideal fields and in the experimental validation section, the directions of fields produced may not necessarily conform to this ideal case. In particular, at higher frequencies, the dimensions of the coaxial structure support more complex modes. This multi-mode propagation starts to occur at a frequency f_m given by $f_m = \frac{c}{\lambda_c} = \frac{c}{\pi\left(\frac{D+d}{2}\right)\sqrt{\mu_R\epsilon_R}}$ where, d and D are the diameter of the inner and outer conductors, respectively. Substituting 0.19 meters for D and 0.088 meters for d and $\mu_R = \epsilon_R = 1$ in the above equation results in f_m = 687 MHz.

At frequencies below f_m the lumped element approximate equivalent circuit for this coax model looks like a lossy transmission line with the addition of C_2 component in parallel with the series resistance R as shown in Figure 2.

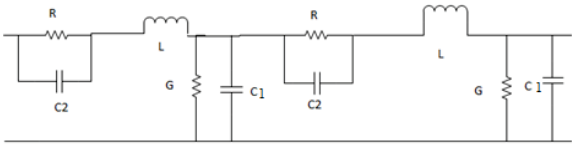

Figure 2. Equivalent circuit of two unit blocks of human body with space suit

The propagation constant can be computed from:

$$\gamma = \alpha + j\beta = \sqrt{\left(\frac{R \times (-jX_{C_2})}{R - jX_{C_2}} + j\,\omega L\right)(G + j\omega C_1)} \qquad (2)$$

where, α is the attenuation constant, β is the phase constant, and R, G, C_1, X_{C2} and L are per unit length values. The conductance G is negligible for air. L and C_1 are based on the expressions for a coax model derived in [6] and they use the values of radius of inner (arm) and outer conductor (space suit) based on our test set up parameters ($b = D/2$= 0.095 and $a = d/2$ = 0.044 meters). The values of L and C_1 are 0.13 uH and 85 pF at 400 MHz. The resistance per unit length R can be calculated from $R = \frac{L}{A\sigma}$ where, L and A are the length and cross-sectional area of a unit block of cylindrical arm model [7] and σ is its conductivity. Similarly, C_2 can be calculated from $C_2 = \frac{\varepsilon_r\varepsilon_0 A}{L}$ where, ε_r is the relative permittivity of human tissue, ε_0 is the permittivity of free space. Table1. shows the relative permittivity and conductivity using Cole-Cole Model with published values in [8].

Estimating the attenuation for arm inside a section of space suit is not easy due to the difficulty of determining the area A in R and C_2 in our inhomogeneous body model. However, we can calculate the upper and lower bounds of the attenuation as explained in the following two subsections.

Table 1 Permittivity and conductivity of human tissues at 400 MHz

Tissue	ϵ_r	$\sigma(S/m)$
Skin	46.787	0.68806
Fat	5.5798	0.04142
Muscle	57.129	0.79631

2.2.1 Equipotential Excitation Assumption along the Cross-sectional Area of Unit Block

Fields within the arm tissue are complex and 3-dimentional in nature. To estimate the values of components in Figure 2 and the resulting attenuation per unit length, we can make a simplifying assumption that the cross-section shown in Figure 3 is an equipotential surface [7]. In this case, the definition of area A in equations for R and C_2 for a certain tissue is the cross-sectional area of that tissue. Namely, the area (A_{tissue}) of skin or fat tissues is the circumference of that tissue multiplied by its corresponding thickness. However, the area A_{tissue} for muscle is approximately the area of a circle representing the muscle with radius equals to the thickness of muscle. Capacitances of skin, fat and muscle layers can be calculated based on the area of each layer and its relative permittivity. Then, the capacitance C_2 in Figure 2 is equivalent to three parallel capacitors. Likewise, R is the equivalent resistance of three parallel resistors each calculated based on the conductivity and (in Table 1) and cross-sectional area of those tissues.

2.2.2 Exciting the Fields on the Surface of Skin

The assumption that the cross-section in Figure 3 is an equipotential surface is only a rough approximation. At sufficiently high frequency, most electric fields propagate in only skin and fat layers. Thus, we calculate the capacitances of skin and fat layers where the area for skin and fat tissues can be calculated in exact way as mentioned in the Equipotential

Excitation subsection. Then, the capacitance C_2 in Figure 2 is the equivalent of only these two parallel capacitors. Similarly, the resistance per unit block R is the equivalent resistance of skin and fat resistors that are in parallel.

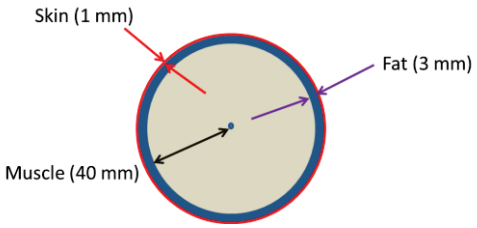

Figure. 3 Human Body model composed of skin, fat and muscle layers

The resulting R and X_{C2} values for the two cases discussed above are provided in Table 2 below.

Table 2 Values of X_{C2}, R per unit block of 1 meter and attenuation for 30 cm unit length

	X_{C2}	R (Ohm)	Attenuation (dB) for 30 cm unit length
Lower Bound (Equipotential Excitation)	147.5	230	2.6
Upper Bound (Excitation on the surface of skin)	2574	4468	50.8

It can be observed from Table 2 that the resistance for the case of equipotential excitation is relatively low. Therefore, this case provides a lower bound on the expected attenuation. However, the values of resistance, reactance and subsequently the attenuation become very high if we assume wave excitation on the surface of skin. This case provides an upper bound on the expected attenuation. In reality, the fields penetrate partially into the muscle region motivating the need for simulations and measurements to better estimate the expected attenuation.

3. SIMULATION AND EXPERIMENTAL VALIDATION OF COAX MODEL

In this part, we use annular rings made of copper fabrics placed 30 cm apart (see Figure 4) on a person's arm to excite transverse electromagnetic (TEM) wave based on the coax model assumption. Ground is tied to the outer conductive cylinder.

3.1 Simulation and Measurement Setup

The numerical simulation is carried out using Agilent's EMPro FDTD based solver to find the forward transmission gain (S21) curve. We simulate the human arm with multilayer cylinders forming the skin, fat and muscle. The thicknesses of the layers used are 1mm, 3mm and 40 mm respectively. Figure 4 shows the simulation model including a human arm and annular rings as well as a tube of aluminum representing the TMG layers in the space suit. Conformal meshing [9] is enabled for the annular rings and aluminum tube so that the meshes for the metal objects can be properly generated. The target cell sizes in the grid regions for skin, fat and muscle tissues are 2 mm, 4mm and 4 mm, respectively. Also, the target cell sizes for the annular rings and aluminum tube are 1mm and 4 mm, respectively. The target base cell size for the entire simulation domain is set to 1 mm in the three dimensions. The boundary conditions for the box containing the model are absorbing boundaries in the 3 dimensions and a perfectly matched layer (PML) is used with 8 layers as type of absorption. The relative permittivity and conductivity values used are based on the Cole-Cole model and frequency-dependent. The simulation timestep is 1.178×10^{-12} seconds which satisfies the stability condition. The maximum simulation time is set to 1,000,000 multiplied by the timestep. However, convergence occurs before that time in our simulations. A transmit power of 0 dBm is applied to one of the annular rings in the frequency range of 300 KHz to 3 GHz. The field of interest converges sufficiently in these conditions. A convergence threshold of -30 dB produces relatively accurate S-parameter curves.

To validate simulations, a measurement is also performed as shown in Figure 4. During the measurement, a human arm is inserted inside a metal tube after wearing two annular rings of copper fabrics separated by 30 cm. These annular rings are then connected to HP Network Analyzer with the ground contacting the outer cylinder.

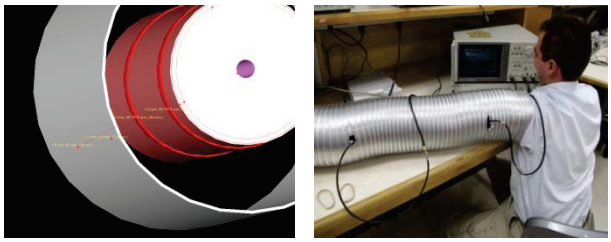

Figure 4. Simulation (left) and Measurement Setup (right)

3.2 Simulation and Measurement Results

The S21 curves for the simulated and measured values are plotted in Figure 5 and Figure 6, respectively. It can be noticed that there is no cutoff frequency in the S21 curves, so waveguide propagation mode is not supported in the presented arm with space suit model. The attenuation of the signal is simulated in Figure 5 for a separation of 30, 60 and 90 cm between the two rings (blue, red and green curves, respectively) but measured only for 30 cm distance due to length constraints on a real arm. We can observe the total simulated loss at 400 MHz is 28.6 dB for 30 cm and 36.5 dB for 60 cm and 45.5 dB for 90 cm distance. On the other hand, the measured total loss at 400 MHz is 31.7 (Figure 6) which is 3.1 dB higher than the simulated loss due to non-ideal measurement setup. In the measurements, there is an impedance discontinuity between the cavity inside the aluminum tube and the impedance of the coaxial feedlines, which results in an extra loss in the S21 curves.

It can be estimated from Figure 5, that the channel loss due to coax mode propagation for 30 cm arm length is the difference between the simulated losses at 60 cm and 30 cm distances, which is around 7.9 dB at 400 MHz. The channel loss for the next 30 cm arm length is around 9 dB. Small fluctuations in the simulations are not significant and the average of these two values is considered a reasonable estimate. Compared to the upper and lower bounds of attenuation discussed in Section 2, the simulated path loss is well within the bounds and the simulated path loss

(attenuation) is closer to the lower bound where equipotential excitation is assumed. This observation suggests that the fields in the tissue penetrate well into the muscle region, which is not surprising especially if we realize that the wave is launched at relatively low frequency (400 MHz) where the penetration/skin-depth of body layers is relatively deep (5.53 cm for skin, 30 cm for fat and 5.2 cm for muscle)

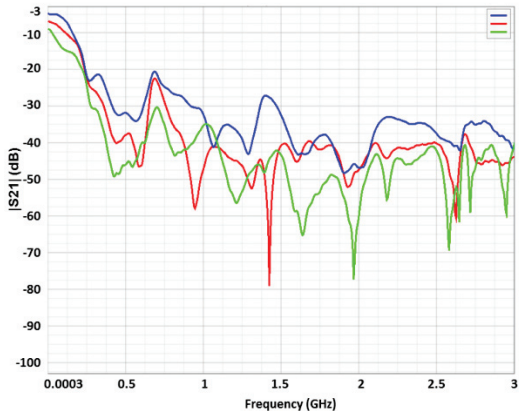

Figure 5. Simulated S21 curve. 300 kHz to 3 GHz. 10 dB/division vertical. (Blue for 30 cm, red for 60 cm and green color for 90 cm distance)

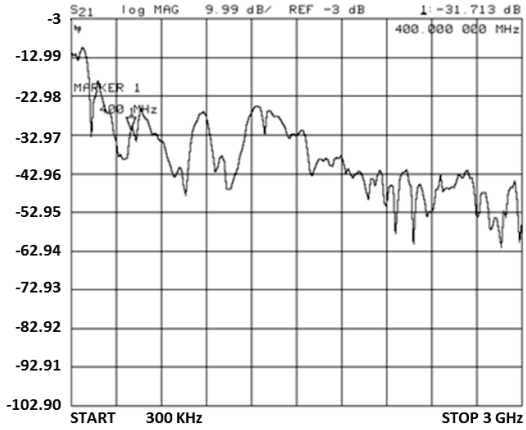

Figure 6. Measured S21 curve. 300 kHz to 3 GHz. ~10 dB/division vertical.

In addition to the channel loss per unit length, additional loss is seen. This loss can be calculated as the difference between the measured total loss for 30 cm distance in Figure 6 (31.7 dB) and the channel loss found for 30 cm arm length (~8.4 dB). The result is 23.3 dB which is in part due to the impedance mismatch at the input and output of the coax mode with the 50 Ohm impedance of the networks analyzer ports. Another reason is the antenna transducer effect of the copper rings (almost quarter wavelength compared to half of the circumference of the rings). The annular rings and ground connections do not perfectly excite the coax mode, so this level of IO port mismatch-attenuation is not surprising.

To get a clear idea about the propagating wave, the directions of electric and magnetic fields are plotted. To do that, using the simulation model in Figure 4 (left), we use a 3D Direct FEM based solver. The initial minimal mesh size is 0.3125 mm and the convergence occurs when delta error is equal to 0.02 where the required consecutive passes of delta error before simulation stops is 2 [10]. To display the fields, a vertical cut plane with arrows representing field directions and strength at distance of 34.5 cm (slightly less than half wavelength at 400 MHz) away from the excitation point is illustrated in Figure 7 and magnetic field in Figure 8. The arrows with red color represent strong field and the blue color represents week field. It is clear that the electric field is normal and the magnetic field is tangential to the human arm. Thus, the structure supports a TEM wave and the coax model works well, especially at lower frequencies.

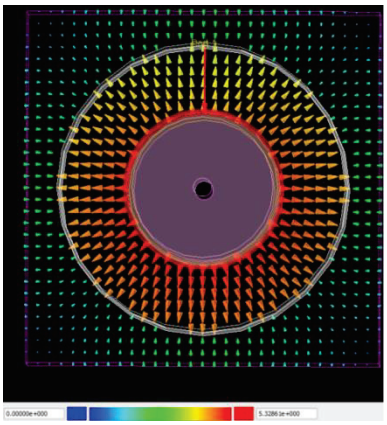

Figure 7. Electric field direction at 34 cm separation

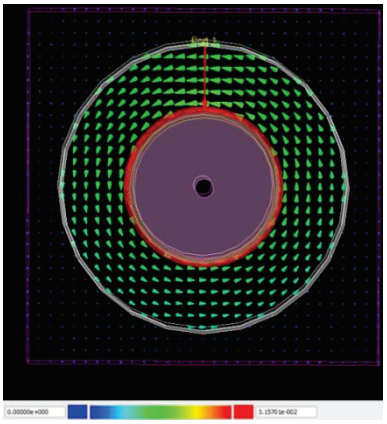

Figure 8. Magnetic field direction at 34 cm separation

4. CONCLUSIONS

In this paper, a coaxial model for signal propagation inside space suits is presented. Simulations show a channel loss value that is well within calculated bounds and the model fits the measured data better than a loaded waveguide model, since no lower cutoff frequency is observed. Future analysis will focus on modeling and estimation of attenuation at locations in the suit where the coaxial diameters change as the signals propagate via different areas of the body (e.g. arm-to-chest cavity transitions), extending the results to a full-suit environment.

5. ACKNOWLEDGMENTS

This research was supported by NASA EPSCoR Program grant number NNX11AM05A. The authors would like to thank NASA for their support.

6. REFERENCES

[1] "Medical Device Radiocommunications Service (MedRadio)," FCC, 26 July 2010. [Online]. Available: http://www.fcc.gov/encyclopedia/medical-device-radiocommunications-service-medradio.

[2] P.S. Hall, Y. Nechayev, Y. Hao, A. Alomainy, M. R.Kamarudin, C.C. Constantinou, R. Dubrovka, and C. G. Parini, "Radio channel characterisation and antennas for on-body communications," in *in Proc. Loughborough Antennas and Propagation*, Loughborough, UK, Apr. 2005, pp. 330-333.

[3] A. Fort, C. Desset, P. De Doncker, P. Wambacq, and L. Van Biesen, "An ultra-wideband body area propagation channel Model-from statistics to implementation," *IEEE Trans. Microw. Theory Tech.,* Vols. 54, no. 6, p. 1820–1826, Jun. 2006.

[4] "Spacesuits and Spacewalks," NASA, [Online]. Available: http://www.nasa.gov/audience/foreducators/spacesuits/home/clickable_suit_nf.html. [Accessed 27 September 2012].

[5] C. A. Balanis, "Circular cross-section waveguides and cavitives," in *Advanced Engineering Electromagnetics* , Wiley , 2011, p. 492.

[6] M. Thompson, "Physics 623 Transmission Lines," University of Wisconsin Madison, 22 Aug 2007. [Online]. Available: http://www.physics.wisc.edu/undergrads/courses/fall2012/623/sn/1-Transmission_Line_notes.pdf.

[7] Namjun Cho; Yoo, J.; Seong-Jun Song; Jeabin Lee; Seonghyun Jeon; Hoi-Jun Yoo, "The Human Body Characteristics as a Signal Transmission Medium for Intrabody Communication," *IEEE Transactions on Microwave Theory and Techniques,* vol. 55, no. 5, pp. 1080,1086, May 2007.

[8] D. Andreuccetti, "Dielectric Properties of Body Tissues," Italian National Research Council, 2010. [Online]. Available: http://niremf.ifac.cnr.it/tissprop/.

[9] "Using Conformal FDTD Meshing," Agilent Technologies , [Online]. Available: http://edocs.soco.agilent.com/display/empro201101/Using+Conformal+FDTD+Meshing. [Accessed 20 Feb 2012].

[10] "Specifying FEM Simulation Setup," Agilent Technologies , [Online]. Available: http://edocs.soco.agilent.com/display/empro2011/Specifying+FEM+Simulation+Setup. [Accessed 5 August 2013].